RT-LAB Platform for Real-Time Implementation of Luenberger Observer Based Speed Sensorless Control of Induction Motor

Submitted: 14th December 2018; accepted: 20th December 2019

Mansour Bechar, Abdeldjebar Hazzab, Mohamed Habbab, Pierre Sicard, Mohammed Slimi

DOI: 10.14313/JAMRIS/4-2019/39

Abstract: *This paper proposes RT-LAB platform for real-time implementation of Luenberger observer based on speed sensorless scalar control of induction motor. The observed shaft speed is derived from lyapunov's theory. It is shown by an extensive study that this Luenberger observer with PI anti-windup speed controller is completely satisfactory at (nominal, variable, reverse) speed references and it is also robust to load torque disturbance. The sensorless control algorithm along with the proposed Luenberger observer is modeled, built in the Host PC and successfully implemented in real-time using digital simulator OP5600. The experimental results observed in the GW-Instek digital oscilloscope's screen validate the effectiveness of the proposed Luenberger observer for speed sensorless scheme.*

Keywords: *Digital simulator (OP5600), induction motor, Luenberger observer, RT-LAB platform, speed sensorless control, PI controller, PI anti-windup controller*

1. Introduction

The three-phase induction motor is one of the most widely used machines in the world due to its high reliability, relatively low cost and modest maintenance requirements [1]. The sensorless control of induction machines in variable speed operation is more complicate than DC machines. The main reasons are that they have more complex dynamics and they more request of complicated calculations.

A high performance sensorless control of AC machine drives require speed information. Generally the mechanical sensors such as shaft encoders or resolvers provide this information [2]. In aggressive environments, the sensor might be the weakest part of the system, thus degrades the system's reliability. This has led to a great many speed sensorless methods.

A lot of senseless control of induction motor strategies have been proposed in the last few years for rotor speed observation. In general, these observers divided into five main schemes: Adaptive Observers [3]. Sliding Mode Technique [4]. Extended Kalman Filter [5]. MRAS observers [6]. Fig. 1 shows a chart of the different speed sensorless estimation strategies:

This paper implements a Luenberger observer for rotor speed estimation using RT-LAB platform. The observer and scalar control models are initially built offline using Matlab/Simulink blocksets and implemented in real-time environment using RT-LAB software and an OP5600 digital simulator. This observer is designed to simultaneously estimate the rotor speed and fluxes also the stator currents, the speed observer stability is ensured through the Lyapunov theory. Experimental validation of the concept is also

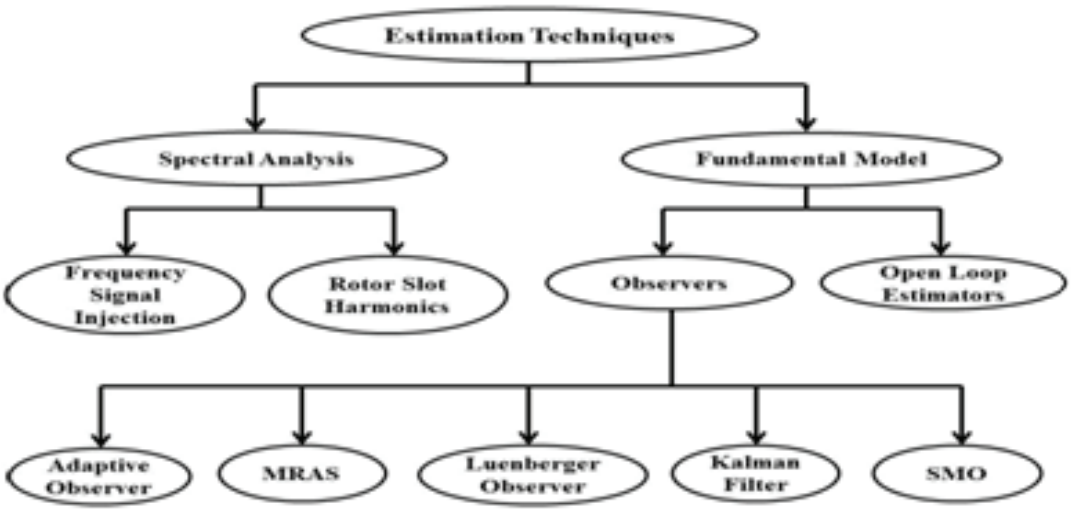

Fig. 1. Speed sensorless estimation strategies

provided in this paper to demonstrate the effectiveness of the proposed sensorless control algorithm with PI anti-windup speed controller at (nominal, variable, reverse) speed references with load disturbance application.

2. Induction Motor Model

The dynamic model of induction motor in two-phase stationary frame with assuming that the stator current and the flux as state variables. It is described as follows [7-8]:

$$\begin{cases} \dfrac{\mathrm{d}i_{s\alpha}}{\mathrm{dt}} = -\dfrac{1}{\sigma.\mathrm{L_s}}\left(\mathrm{R_s}+\left(\dfrac{\mathrm{L_m}}{\mathrm{L_r}}\right)^2.\mathrm{R_r}\right).i_{s\alpha}+\dfrac{\mathrm{L_m}.\mathrm{R_r}}{\sigma.\mathrm{L_s}\mathrm{L_r^2}}\varphi_{r\alpha} \\ +\dfrac{\mathrm{L_m}}{\sigma.\mathrm{L_s}\mathrm{L_r}}w_r.\varphi_{r\beta}+\dfrac{1}{\sigma\mathrm{L_S}}V_{s\alpha} \\ \dfrac{\mathrm{d}i_{s\beta}}{\mathrm{dt}} = -\dfrac{1}{\sigma.\mathrm{L_s}}\left(\mathrm{R_s}+\left(\dfrac{\mathrm{L_m}}{\mathrm{L_r}}\right)^2.\mathrm{R_r}\right)i_{s\beta}-\dfrac{\mathrm{L_m}}{\sigma.\mathrm{L_s}\mathrm{L_r}}w_r.\varphi_{r\alpha} \\ +\dfrac{\mathrm{L_m}.\mathrm{R_r}}{\sigma.\mathrm{L_s}\mathrm{L_r^2}}\varphi_{r\beta}+\dfrac{1}{\sigma.\mathrm{L_s}}V_{s\beta} \\ \dfrac{\mathrm{d}\varphi_{r\alpha}}{\mathrm{dt}} = \dfrac{\mathrm{L_m}.\mathrm{R_r}}{\mathrm{L_r}}i_{s\alpha}-\dfrac{\mathrm{R_r}}{\mathrm{L_r}}\varphi_{r\alpha}-w_r.\varphi_{r\beta} \\ \dfrac{\mathrm{d}\varphi_{r\beta}}{\mathrm{dt}} = \dfrac{\mathrm{L_m}.\mathrm{R_r}}{\mathrm{L_r}}i_{s\beta}+w_r.\varphi_{r\alpha}-\dfrac{\mathrm{R_r}}{\mathrm{L_r}}\varphi_{r\beta} \end{cases} \quad (1)$$

where: $i_{s\alpha}$, $i_{s\beta}$ are stator current vector components in [α,β] stator coordinate system, $V_{s\alpha}$, $V_{s\beta}$ are stator voltage vector components in [α,β] stator coordinate system, $\varphi_{r\alpha}$, $\varphi_{r\beta}$ are rotor magnetic flux in [α, β] stator coordinate system, L_m is magnetizing inductance, L_r is rotor inductance, L_s is stator inductance, R_r is rotor resistance, R_s is stator resistance, w_r is rotor angular speed, σ is leakage coefficient $\sigma = 1-\dfrac{\mathrm{L_m^2}}{\mathrm{L_r}.\mathrm{L_s}}$, P is poles number, $T_r = \dfrac{\mathrm{L_r}}{\mathrm{R_r}}$ the rotor time constant.

The electromagnetic torque can be expressed by:

$$T_e = \frac{3.\mathrm{P}.\mathrm{L_m}}{2.\mathrm{L_r}}.(\varphi_{r\alpha}.i_{s\beta}-\varphi_{r\beta}.i_{s\alpha}) \quad (2)$$

3. Design of Luenberger Observer

The Luenberger observer, which estimates states of the system (stator current and rotor flux components), is described by the following equations:

$$\begin{cases} \dot{\hat{X}} = A\hat{X}+BU+L(Y-C\hat{X}) \\ \hat{Y} = C\hat{X} \end{cases} \quad (3)$$

Where $\hat{X} = [\hat{i}_{s\alpha}\ \hat{i}_{s\beta}\ \hat{\varphi}_{r\beta}]^{\mathrm{T}}$; $U = [V_{s\alpha}\ V_{s\beta}]^{\mathrm{T}}$; $Y = [i_{s\alpha}\ i_{s\beta}]^{\mathrm{T}}$; $\hat{Y} = [\hat{i}_{s\alpha}\ \hat{i}_{s\beta}]^{\mathrm{T}}$.

The symbol ^ denotes the estimated values, $\hat{\mathrm{X}}(\mathrm{t})$ is the vector of the states to be estimated and $\hat{\mathrm{Y}}$ is the vector with the desired outputs. L is the observer gain matrix, which is selected so that the system will be stable. The estimation error of the system sates (stator current and rotor flux components) may be obtained by:

$$\dot{e} = (A-LC)e+(\Delta A)\hat{X} \quad (4)$$

in which ΔA can be simply expressed as:

$$\Delta A = A(w_r)-A(\hat{w}_r) = \begin{bmatrix} 0 & 0 & 0 & \dfrac{\mathrm{L_m}}{\sigma.\mathrm{L_s}\mathrm{L_r}}\Delta w_r \\ 0 & 0 & -\dfrac{\mathrm{L_m}}{\sigma.\mathrm{L_s}\mathrm{L_r}}\Delta w_r & 0 \\ 0 & 0 & 0 & -\Delta w_r \\ 0 & 0 & \Delta w_r & 0 \end{bmatrix} \quad (5)$$

where: $\Delta w_r = w_r - \hat{w}_r$ is the rotor speed error and

$$e = X - \hat{X} = \begin{bmatrix} \mathrm{e}_{i_{s\alpha}} & e_{i_{s\beta}} & e_{\ddot{o}_{r\alpha}} & e_{\ddot{o}_{r\beta}} \end{bmatrix}^T \quad (6)$$

is the state estimation error, we should consider the following Lyapunov function to obtain the adaptive speed estimation scheme [9]:

$$V = e^T e+\frac{(\Delta w_r)^2}{\lambda} \quad (7)$$

where λ is a positive constant. By deriving the expression (7) in relation to time, gives:

$$\dot{V} = \left\{\frac{d(e^T)}{dt}\right\}e+e^T\left\{\frac{d(e)}{dt}\right\}+\frac{1}{\lambda}\ \frac{d}{dt}(\Delta w_r)^2 \quad (8)$$

$$\dot{V} = e^T\left\{(A-LC)^T+(A-LC)\right\}.e$$

$$-2\frac{\mathrm{L_m}}{\sigma.\mathrm{L_s}\mathrm{L_r}}\Delta w_r(\mathrm{e}_{i_{s\alpha}}\hat{o}_{r\beta}-\mathrm{e}_{i_{s\beta}}\hat{o}_{r\alpha})$$

$$+\frac{2}{\lambda}\Delta w_r\frac{d}{dt}\hat{w}_r \quad (9)$$

The adaptation law for the estimation of the rotor speed can be deduced as:

$$\hat{w}_r = \lambda\frac{\mathrm{L_m}}{\sigma\mathrm{L_s}\mathrm{L_r}}\int_0^t(\mathrm{e}_{i_{s\alpha}}\hat{\varphi}_{r\beta}-\mathrm{e}_{i_{s\beta}}\hat{\varphi}_{r\alpha})dt \quad (10)$$

The speed is estimated by a PI controller described as:

$$\hat{w}_r = K_P(e_{is\alpha}\hat{\varphi}_{r\beta}-e_{is\beta}\hat{\varphi}_{r\alpha})+$$
$$K_i\int(e_{is\alpha}\hat{\varphi}_{r\beta}-e_{is\beta}\hat{\varphi}_{r\alpha}).dt \quad (11)$$

where K_p and K_i are the proportional and integral terms of the adaptive scheme. The feedback gain matrix L is chosen to ensure the fast and dynamic performance of closed loop observer [10-11]:

$$L = \begin{bmatrix} L_1 & -L_2 \\ L_2 & L_1 \\ L_3 & -L_4 \\ L_4 & L_3 \end{bmatrix} \quad (12)$$

with L_1, L_2, L_3 and L_4 are given by:

$$\begin{cases} L_1 = (k-1)\left(\dfrac{1}{\sigma.T_s} + \dfrac{1}{\sigma.T_r}\right) \\ L_2 = -(k-1).\hat{w}_r \\ L_3 = (k^2-1).\left\{\left(\dfrac{1}{\sigma.T_s} + \dfrac{1}{\sigma.T_r}\right)\dfrac{\sigma.\mathrm{L_s}.\mathrm{Lm}}{\mathrm{L_r}} - \dfrac{\mathrm{Lm}}{\mathrm{T_r}}\right\} \\ \quad + \dfrac{\sigma.\mathrm{L_s}.\mathrm{Lm}}{\mathrm{L_r}}\left(\dfrac{1}{\sigma.T_s} + \dfrac{1}{\sigma.T_r}\right)(k-1) \\ L_4 = -(k-1)\dfrac{\sigma.\mathrm{L_s}.\mathrm{Lm}}{\mathrm{L_r}}.\hat{w}_r \end{cases} \tag{13}$$

where k is a positive coefficient obtained by pole placement approach [12]. A block diagram illustrating the behavior of the observer is shown in Fig. 2.

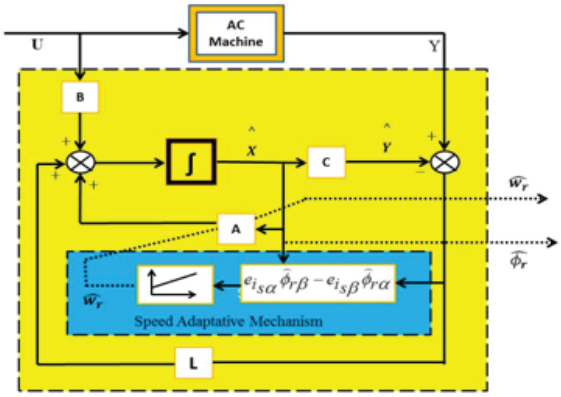

Fig. 2. Block diagram of the proposed Luenberger observer

4. Sensorless Scalar Control Scheme

The scalar control (Volt/Hertz) is a simple technique used to control induction motors speed in both open and closed loop. However, its dynamic performance is limited, even in closed loop, particularly when operating in regions of low speed [13].

The main concept is to keep the ratio between voltage and frequency constant to maintain available torque constant. If the voltage does not have a proper relationship with the frequency. The machine can operate in the saturation or field weakening region [14]. From the relationship between the electromagnetic flux and stator voltage the stator pulsation is deduced, expressed as:

$$s \quad \omega_s * \varphi_s * \sqrt{\frac{\left(\dfrac{R_s}{\omega_s.L_s} - \omega_r.T_r.\sigma\right)^2 \left(1 + \left(\omega_r.T_r.\dfrac{R_s}{\omega_s.L_s}\right)\right)^2}{(\omega_r.\ _r.\sigma)}} \tag{14}$$

Indeed, in practice, we are usually satisfied with a simplified control law, corresponding to the negligence of the ohmic drop (Rs = 0) in (14), to give us:

$$V_s = \omega_s * \varphi_s \tag{15}$$

The block diagram of sensorless scalar control of induction motor is shown in Fig. 3, the real-time implementations of Luenberger observer and control algorithm are evaluated by RT-LAB platform.

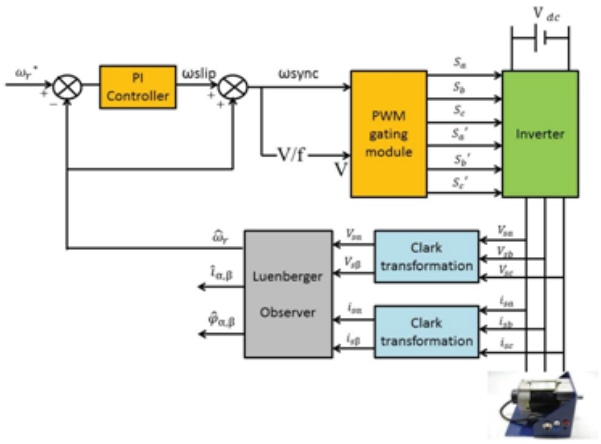

Fig. 3. Block diagram of sensorless scalar control of induction motor

5. Real-Time Platform Using RT-LAB

RT-LAB platform for validation of the proposed controller and observer is shown in Fig. 4, this platform was built using RT-LAB as real-time Platform, and it contains OP-5600 OPAL-RT real-time simulator used as a core of the hardware prototype system. Currently, CAOSEE Laboratory at Bechar University is equipped with one OP5600 OPAL-RT Simulator and one

Drivelab OPAL-RT Board [15]. The scalar control algorithm and Luenberger observer are created in Matlab/Simulink software on the RT-LAB host computer with two subsystems SM and SC, the SM subsystem is converted into 'C' source code using Mathworks code generator Real-Time-Workshop (RTW) and compiled using RT-LAB. This code is then uploaded into the OP5600 target via network connections TCP/IP protocol.

The test bench is shown in Fig. 4 that is composed of:

(1) Squirrel cage induction motor with the following characteristics: Δ-connected, four poles, 125 W, 4000 rpm, 30 V, 133 Hz with the 1024 points integrated incremental coder,
(2) DC generator motor,
(3) Resistive load,
(4) Inverter Drivelab Board,
(5) Hall type current sensors, voltage sensors,
(6) Auto transformer (0-450 V),
(7) OP5600 real-time digital simulator with Host computer equipped by RT-LAB software,
(8) Numerical oscilloscope.

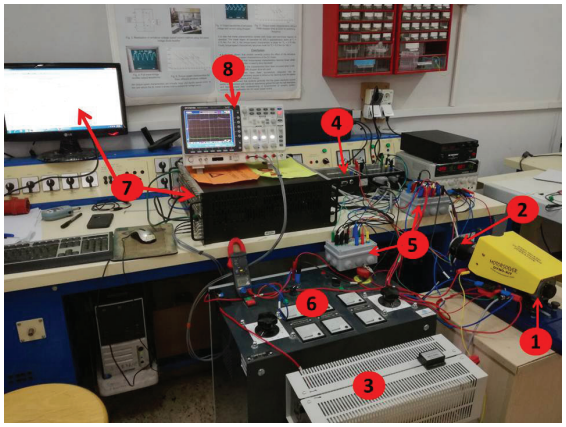

Fig. 4. A hardware prototype system based on the RT-LAB platform

The OP5600 real-time digital simulator has two main sections (upper section containing analog and digital I/O signal modules and bottom section containing one CPU with four cores Intel XeonQuadCore 2.40 GHz able to send and receive various digital and analog signals via Xilinx Spartan-3 FPGA I/O card FPGA Board).

Now the Simulink model is executed via RT-LAB software and it is made compatible for real-time control. RT-LAB model contains two subsystems as depicted in Fig. 5, the console subsystem (SC) contains user interface blocks such as scopes and controls. It allows user to monitor the system completely while the simulation is running in real-time. On other hand, all the computational elements are included in master subsystem (SM), when executing the model in real-time the subsystem that contains the calculation part does not require any change because it is running on the simulator.

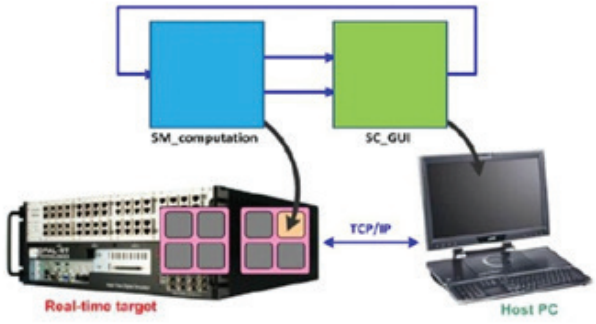

Fig. 5. RT-LAB model for real-time control

The analog-in block is used to transfer external sensed voltage and current signals (Ia,Ib,Ic and Va,Vb,Vc) from current sensors and voltage sensors into the real-time control environment. Each analog-in and digital-in block can be used to access eight analog or digital signals. The sensed analog signals are applied to the analog-in card (Slot 1 Module B subsection 1) as shown in Fig. 6. The digital signal sensed from encoder sensor signal is applied to the digital-in card (slot 2 Module A subsection 1). The digital-out block is required to transfer real-time simulation signals from OP5600 simulator to the outside world. The signals exchanged between the OP5600 simulator and drivelab board in the range of (+/-5~+/-20) V.

Which can be implemented by A/D converters or D/A converters with acceptable accuracy [16]. The digital-out card provides digital output signals with specific voltage conditioning. The galvanic isolation of the digital-out card outputs make it ideal for environments, where voltage isolation is required. A push-pull transistor isolated output can sink up to 50 mA continuous, and up to +30 V applied at pin 18 of DB37 connectors this DC voltage defined according to user requirements.

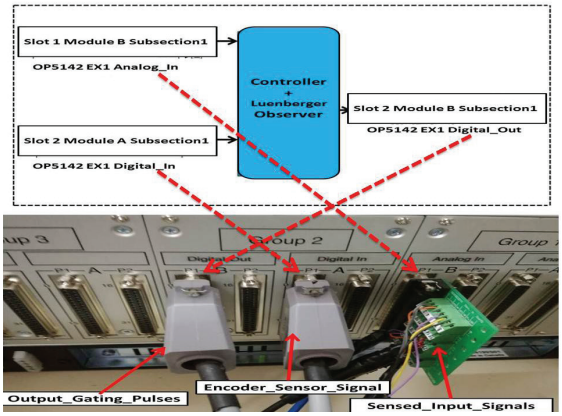

Fig. 6. OP5600 rear view

Finally, the scalar control algorithm and Luenberger observer are simulated on a real-time digital simulator OP5600 using one of a dual-quad computer. The gating pulses available at digital-out (slot 2 module B subsection 2) are applied to the inverter switches (MOSFETs) through gate driver circuit.

6. Experimental Results

The performance of current estimator and closed loop speed estimator are tested in our experimental setup, the different waveforms are given those are obtained from digital oscilloscope with 4 channels. The sampling time for the acquisitions and for the calculation has been set at 400 µs.

6.1. PI Controller

In this case the proportional-integral (PI) controller is used for speed regulation. Fig. 7 shows the PI diagram.

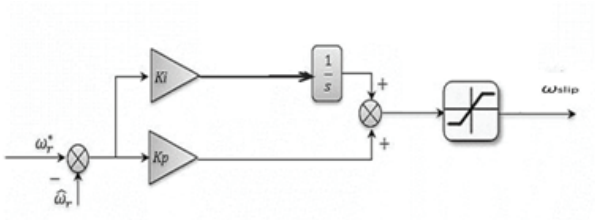

Fig. 7. Structure of PI controller adopted in speed loop control

First the motor is started under no load with nominal speed of 350 rad/sec, and after 2.5 sec, a rated load is applied, in 11 sec the motor is unloaded again.

Fig. 8 shows the behavior of induction motor at nominal speed with disturbance load application. The reference speed is set to 350 rad/sec. it is clear that the PI controller exhibits good performances at steady state but in dynamic regime, when the motor started up the PI controller exceed the saturation value and generate inadequate performances to the system as a large overshoot and a long settling time as shown in Fig. 8.

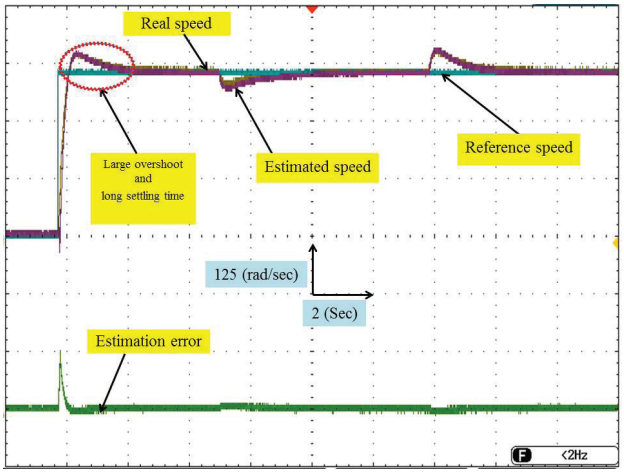

Fig. 8. The reference, real and estimated speed, with estimation error

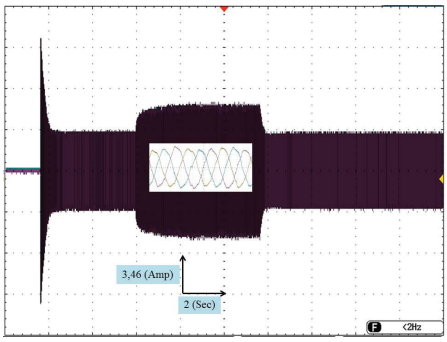

Fig. 9. Stator currents: i_a, i_b, i_c [A]

It can be also seen that the observed speed tracks the real speed even the load is applied, the estimation error between the two speeds is approximately neglected in steady state but this error increased at starting time.

Fig. 11 shows the measured and observed currents, the observed currents $\hat{i}_{s\alpha}, \hat{i}_{s\beta}$ track the measured currents $i_{s\alpha}$, $i_{s\beta}$. It can be seen that the current waveforms are practically sinusoidal with low total harmonic distortion (THD= 53.20%) shown in Fig. 12.

Fig. 13 shows the estimated rotor flux components. So, globally it can be seen from these results that the performances of the proposed Luenberger observer are satisfactory with PI speed controller.

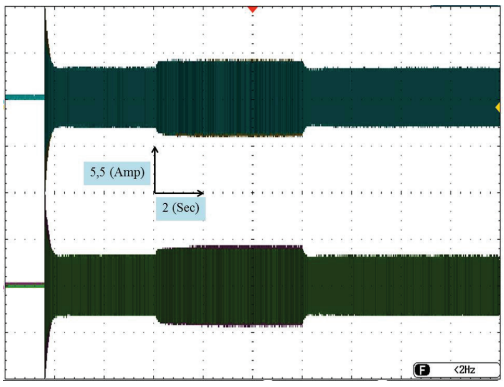

Fig. 10. Real and estimated current components $i_{s\alpha}$, $i_{s\beta}$, $\hat{i}_{s\alpha}$, $\hat{i}_{s\beta}$

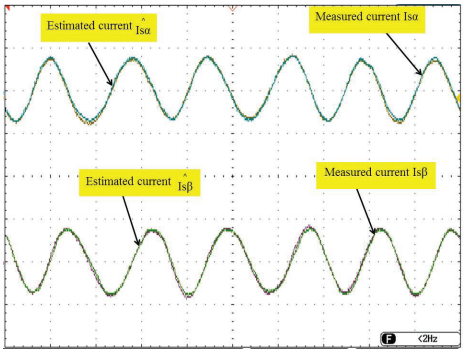

Fig. 11. Zoom of real and estimated current components $i_{s\alpha}$, $i_{s\beta}$, $\hat{i}_{s\alpha}$, $\hat{i}_{s\beta}$

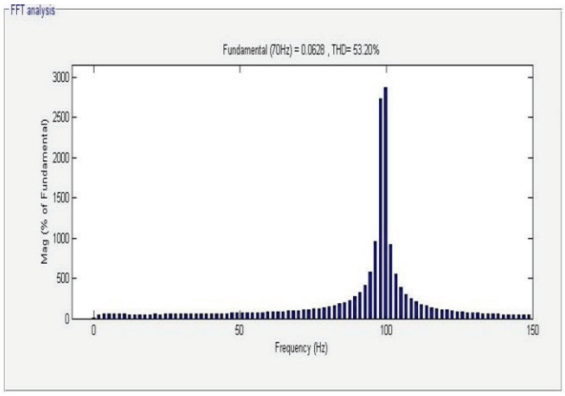

Fig. 12. FFT analysis and spectrum of THD for stator phase current $i_{s\alpha}$

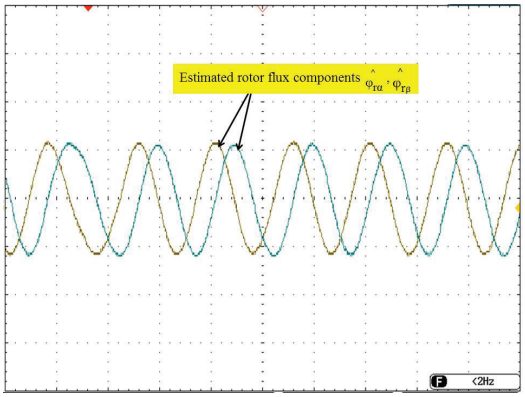

Fig. 13. Zoom of Estimated rotor flux components $\hat{\varphi}_{r\alpha}$, $\hat{\varphi}_{r\beta}$

6.2. Anti-windup PI Controller

When occurs a large step change in the speed reference PI controller usually disregarding the physical limitation of the system so this phenomenon known by integrator windup that generate inadequate performances as shown in fig.8 a large overshoots , long settling time about 2 sec. Thus an anti-windup technique is used in this situation by cancelling the wind up phenomenon which is caused by the saturation of the pure integrator [17]. Fig. 14 shows the speed anti-windup PI controller diagram block, where Ti is tracking time constant gain.

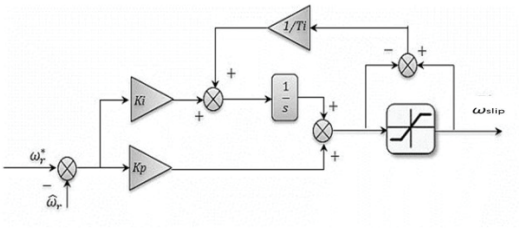

Fig. 14. Structure of anti-windup PI controller adopted in speed loop control

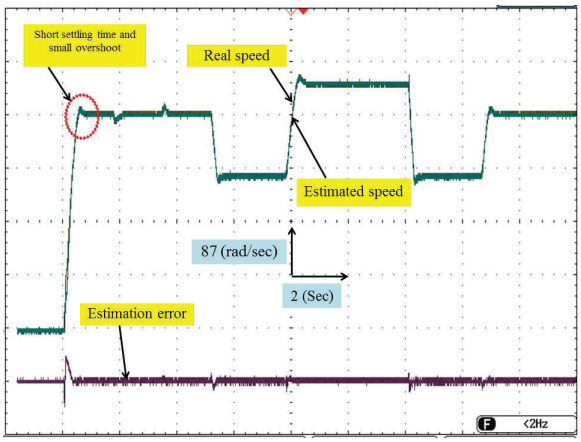

Fig. 15. Rotor speed estimation under variable speed reference with estimation error

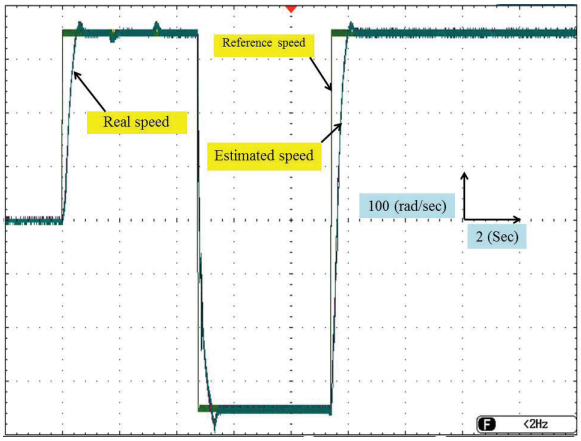

Fig. 16. Speed sense reversing: estimated and real speeds

Speed variation test (3343, 2388, 3822, 3343 rpm) in Fig. 15, the anti-windup PI controller rejects the load disturbance very rapidly compared with the PI controller, Fig. 16 rotor speed sense reversing (3343, –3343, 3343 rpm) the anti-windup PI provide perfect superposition and better tracking than PI by reducing the overshoot and settling time. Fig. 17 shows speed estimation error, always converge to zero, that is indicate the effectiveness of the proposed luenberger speed observer.

Generally the performances of the proposed observer have been verified experimentally by comparative study between the classical PI controller and anti-windup PI. The next Table 1 summarizes the comparative analysis of speed controllers.

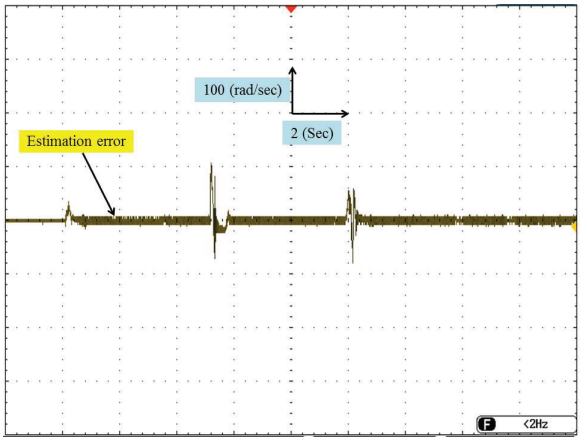

Fig. 17. Speed estimation error

Tab. 1. Comparative analysis between PI and anti-windup PI controller

PI anti-windup PI		
Rise time [sec]	0.53	0.53
Maximum overshoot [%]	7.14	2.28
Settling time [sec]	2	0.8
Speed dropping due to the load application [%]	5.36	2.5

7. Conclusion

In this paper, we have validated the Luenberger observer based speed sensorless control of induction motor using RT-LAB platform. The overall controllers and speed observer were simulated in real-time with time-step 4μs on one core of a 4 cores, including digital and analog I/O access time. The experimental results obtained with PI anti-windup controller show good performances in both dynamic and steady state, with fast load disturbance rejection compared with the results obtained with PI controller. The efficiency of the designed observer allows us to conclude that the speed sensor can be eliminated and replaced by Luenberger observer to reduce the cost of the control system.

The proposed technique was implemented successfully in real-time with assumption that the induction motor parameters values are constants (Tab. 2), but in fact during the very low speed operation the induction motor temperature rise and generated loss-

es (stator copper losses and rotor losses) affects the induction motor parameters, the speed observer performances are disregarding also, so further research is open to test the observer robustness against parameters variation in real-time.

Tab 2. Induction motor parameters

P_n [W]	120	R_s [Ω]	1.05
ω_n [min^{-1}]	4000	R_r [Ω]	1.705
P	2	L_s [H]	0.02939
J [kg/m^2]	0.00037	L_r [H]	0.02939
f_c [SI]	0.00006	L_m [H]	0.02526

ACKNOWLEDGEMENTS

The authors thank Tahri Mohammed University and CAOSEE laboratory for all helps and supports.

AUTHORS

Mansour Bechar* – Laboratory of Research Control Analysis and Optimization of Electro-Energetic Systems, Tahri Mohammed University, Bechar, Algeria, E-mail: mansourbechar@gmail.com.

Abdeldjebar Hazzab – Laboratory of Research Control Analysis and Optimization of Electro-Energetic Systems, Tahri Mohammed University, Bechar, Algeria.

Mohamed Habbab – Laboratory of Research Control Analysis and Optimization of Electro-Energetic Systems, Tahri Mohammed University, Bechar, Algeria.

Mohammed Slimi – Laboratory of Research Control Analysis and Optimization of Electro-Energetic Systems, Tahri Mohammed University, Bechar, Algeria.

Pierre Sicard – Group de Recherche en Electronique Industrielle (GREI) Université du Québec à Trois-Rivières C.P.500, Trois-Rivières (Québec), Canada.

* Corresponding author

REFERENCES

[1] A. Abbou, T. Nasser, H. Mahmoudi, M. Akherraz, A. Essadki, "Induction Motor Controls and Implementation using dSPACE", *WSEAS Transactions on Systems and Control*, vol. 7, no. 1, 2012, 26–35.

[2] J. Holtz, "Sensorless control of induction motor drives", *Proceedings of the IEEE*, vol. 90, no. 8, 2002, 1359–1394
DOI: 10.1109/JPROC.2002.800726.

[3] H. Kubota, K. Matsuse, "Speed sensorless field-oriented control of induction motor with rotor resistance adaptation", *IEEE Transactions on Industry Applications*, vol. 30, no. 5, 1994, 1219–1224
DOI: 10.1109/28.315232.

[4] T. Chern, J. Chang, K. Tsai, "Integral-variable-structure-control-based adaptive speed estimator and resistance identifier for an induction motor", *International Journal of Control*, vol. 69, no. 1, 1998, 31–48
DOI: 10.1080/002071798222910.

[5] Y. Kim, S. Sul, M. Park, "Speed sensorless vector control of induction motor using extended Kalman filter", *IEEE Transactions on Industry Applications*, vol. 30, no. 5, 1994, 1225–1233
DOI: 10.1109/28.315233.

[6] C. Schauder, "Adaptive speed identification for vector control of induction motors without rotational transducers", *IEEE Transactions on Industry Applications*, vol. 28, no. 5, 1992, 1054–1061
DOI: 10.1109/28.158829.

[7] G. Tarchała, T. Orłowska-Kowalska, "Sliding Mode Speed Observer for the Induction Motor Drive with Different Sign Function Approximation Forms and Gain Adaptation", *Przegląd Elektrotechniczny*, vol. 89, no. 1a, 2013.

[8] I. Bendaas, F. Naceri, "A new method to minimize the chattering phenomenon in sliding mode control based on intelligent control for induction motor drives", *Serbian Journal of Electrical Engineering*, vol. 10, no. 2, 2013, 231–246
DOI: 10.2298/SJEE130108001B.

[9] J. Maes, J. Melkebeek, "Speed-sensorless direct torque control of induction motors using an adaptive flux observer", *IEEE Transactions on Industry Applications*, vol. 36, no. 3, 2000, 778–785
DOI: 10.1109/28.845053.

[10] D. Casadei, G. Serra, A. Tani, L. Zarri, F. Profumo, "Performance analysis of a speed-sensorless induction motor drive based on a constant-switching-frequency DTC scheme", *IEEE Transactions on Industry Applications*, vol. 39, no. 2, 2003, 476–484
DOI: 10.1109/TIA.2003.808937.

[11] B. Akin, "State estimation techniques for speed sensorless field oriented control of induction motors", M.Sc. Thesis, Middle East Technical University METU, 2003.

[12] S. Ao, L. Gelman, *Advances in Electrical Engineering and Computational Science*, Springer, 2009
DOI: 10.1007/978-90-481-2311-7.

[13] B. K. Bose, *Modern Power Electronics and AC Drives*, Prentice Hall, 2001.

[14] M. Suetake, I. N. da Silva, A. Goedtel, "Embedded DSP-Based Compact Fuzzy System and Its Application for Induction-Motor *V/f* Speed Control", *IEEE Transactions on Industrial Electronics*, vol. 58, no. 3, 2011, 750–760
DOI: 10.1109/TIE.2010.2047822.

[15] M. Bechar, A. Hazzab, M. Habbab, "Real-Time scalar control of induction motor using RT-Lab software". In: *2017 5th International Conference on Electrical Engineering – Boumerdes (ICEE-B)*, 2017
DOI: 10.1109/ICEE-B.2017.8192002.

[16] S. T. Cha, Q. Wu, A. H. Nielsen, J. Østergaard, I. K. Park, "Real-Time Hardware-In-The-Loop

(HIL) Testing for Power Electronics Controllers". In: *2012 Asia-Pacific Power and Energy Engineering Conference*, 2012, 1–6 DOI: 10.1109/APPEEC.2012.6307219.

[17] D. Zhang, H. Li, E. Collins, "Digital Anti-Windup PI Controllers for Variable-Speed Motor Drives Using FPGA and Stochastic Theory", *IEEE Transactions on Power Electronics*, vol. 21, no. 5, 2006, 1496–1501 DOI: 10.1109/TPEL.2006.882342.